Fcc-bcc transition for Yukawa interactions determined by applied strain deformation

Robert S. Hoy* and Mark O. Robbins
Department of Physics and Astronomy, Johns Hopkins University, Baltimore, Maryland 21218, USA
(Received 31 December 2003; published 6 May 2004)

Calculations of the work required to transform between bcc and fcc phases yield a high-precision bcc-fcc transition line for monodisperse point Yukawa (screened-Coulomb) systems. Our results agree qualitatively but not quantitatively with recently published simulations and phenomenological criteria for the bcc-fcc transition. In particular, the bcc-fcc-fluid triple point lies at a higher inverse screening length than previously reported.

DOI: 10.1103/PhysRevE.69.056103 PACS number(s): 64.60−i, 52.27.Lw, 82.70.Dd

I. INTRODUCTION

The screened-Coulomb or Yukawa pair potential $U(r) = \Phi e^{-\kappa r}/r$ has been the focus of great theoretical interest for two reasons. One is that it describes a wide range of interactions, changing continuously from a pure Coulomb potential to an effective hard-sphere potential as the inverse screening length κ increases. The second is that it provides an approximate description of the effective interactions between large ions that are screened by more mobile counterions. In this context it has been used to describe the interactions between ions surrounded by electrons in metals [1], dust grains surrounded by electrons in dusty plasmas [2–4], and macroions surrounded by counterions in charge-stabilized colloidal suspensions [4–8].

The phase diagram of systems of particles interacting with a Yukawa potential has been studied with both analytic [9–14] and numerical [14–24] techniques and compared to experiments on dusty plasmas [25,26] and colloidal suspensions [27–29]. The high-temperature phase is a fluid. There is no liquid-gas transition because the interactions are purely repulsive. The stable crystalline phase at zero temperature changes from bcc to fcc as κ increases. The higher entropy of the bcc phase leads to a greater range of stability as temperature increases until the melting line is reached. Previous results for the fcc-bcc transition line [11,20–24] vary substantially and the most recent detailed calculation [23] quotes an uncertainty of about 10% roughly halfway between the zero-temperature transition point and the triple point.

In this paper we use a different approach to obtain the bcc-fcc phase boundary with an uncertainty of only about 1%. Bounds on the free energy difference between the two phases are obtained by calculating the work done during a continuous deformation between them. The effect of deformation rate, truncation of the potential, and system size and geometry are all analyzed to determine systematic errors. The resulting bcc-fcc transition line is in qualitative agreement with recent simulation results, and quantitative differences are comparable to the larger error bars quoted by previous studies. We estimate the location of the bcc-fcc-fluid triple point using previously published melting-line results [17,23], and find that it lies at higher inverse screening lengths than previously reported.

The role of anharmonicity in stabilizing the fcc phase is analyzed in detail. While anharmonicity increases the energy of the fcc phase relative to that of the bcc, there is an even larger increase in the relative entropic contribution to the free energy that increases the range of stability of the fcc phase. This appears to reflect an increase in the frequency of the long wavelength shear modes that dominate the bcc entropy in the harmonic approximation [21].

Our results are also compared to phenomenological criteria proposed by Vaulina *et al.* [10]. These authors predict a transition at a critical value of the mean-squared displacement about lattice sites, and calculate the displacement using a simple Einstein-like model. We find that the actual displacement from molecular dynamics (MD) simulations on our transition line is in reasonable agreement with their phenomenological criterion, but substantially larger than predicted by their Einstein model.

The details of our calculations are presented in the following section. Sec. III provides a detailed analysis of systematic errors and presents our results for the phase boundary. In Sec. IV, we compare our results to previous transition lines, and Sec. V provides a summary and conclusions.

II. METHOD

A. Free energy difference calculations

Constant number N, volume V, and temperature T (N-V-T) ensembles are most natural for the study of Yukawa systems for two reasons. First, since the Yukawa potential is purely repulsive, the macroions in an experiment will expand to fill the container. Second, the inverse screening length κ is density dependent in charged colloidal suspensions and dusty plasmas [30]. This density dependence is system specific, and affects the pressures and bulk moduli. Thus any calculation of coexistence regions will be nonuniversal. For this reason we focus on finding the Helmholtz free energy difference $\Delta F = F_{fcc} - F_{bcc}$ at fixed volume. Brief discussions of coexistence are given in Secs. II B and III D

Postma, Reinhardt, and others [31–33] have shown that the free energy difference between two phases of a system may be calculated in numerical simulations by evaluating the external work done on the system along a thermodynamic path connecting the phases. From elementary thermodynamics, the mechanical work W_{AB} done on a system on an iso-

*Electronic address: robhoy@pha.jhu.edu

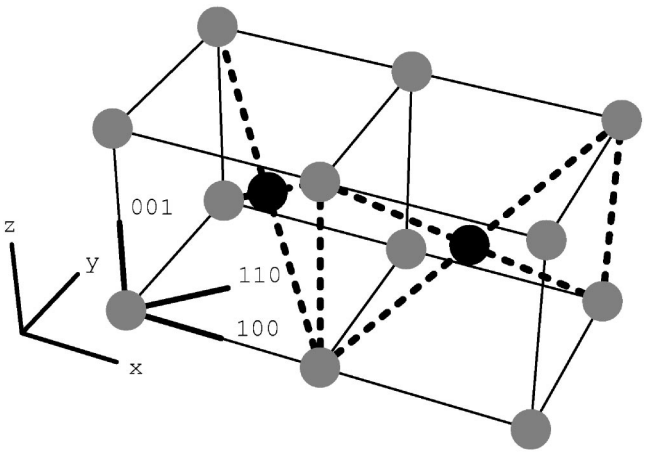

FIG. 1. The Bain transformation. Two cells of a bcc lattice are shown with lattice directions. The body-center atoms are shown in black. When the x, y, and z directions are scaled by $(2^{-1/6},2^{-1/6},2^{1/3})$, the crystal is transformed into an fcc lattice of the same density. The atoms connected by the dotted lines become two (100) faces of an fcc unit cell.

thermal path from state A to state B gives an upper bound on the change $\Delta F_{AB}=F_B-F_A$ in the system's Helmholtz free energy [34]. The work W_{BA} done on the system during the reverse process $B\rightarrow A$ is an upper bound on ΔF_{BA}, and hence $(-W_{BA})$ is a lower bound on ΔF_{AB}.

Bounds on ΔF for Yukawa systems can be obtained using a continuous constant-volume Bain deformation path (Fig. 1) connecting the bcc and fcc lattices. An initially bcc lattice deformed such that its three cubic symmetry directions are scaled, respectively, by $(\zeta^{-1/2},\zeta^{-1/2},\zeta)$ is transformed into an fcc lattice of the same density as ζ varies continuously from 1 to $2^{1/3}$ [35]. We calculate the work done along this path in the forward and reverse directions using strain-controlled molecular dynamics simulations [36].

Assuming that the systems traverse these paths homogeneously, we can calculate the work done from the global stresses and strains. We define

$$W_{bf}=V\int_{bcc}^{fcc}\overline{\sigma}\cdot d\overline{\epsilon}, \tag{1}$$

$$W_{fb}=V\int_{fcc}^{bcc}\overline{\sigma}\cdot d\overline{\epsilon}, \tag{2}$$

where $\overline{\sigma}$ and $\overline{\epsilon}$ are the stress and true strain tensors. W_{bf} and $(-W_{fb})$ are upper and lower bounds on ΔF. For these bounds to be narrow, the intermediate configurations of our systems must remain statistically representative of the ζ-dependent equilibrium distributions as ζ is varied [31]. In particular, the stress tensor $\overline{\sigma}(\zeta)$ must remain near its equilibrium value.

B. Potential parameters

The phase behavior of Yukawa systems is most conveniently expressed in terms of dimensionless screening and temperature parameters. One natural, phase-independent length scale is $a=n^{-1/3}$, where $n=N/V$ is the macroion number density. The Yukawa potential may then be expressed as

$$U(r)=\frac{\Phi}{a}\frac{e^{-\lambda r/a}}{r/a}, \tag{3}$$

where $\lambda=\kappa a$ is the dimensionless screening parameter. The limits $\lambda\rightarrow 0$ and $\lambda\rightarrow\infty$ correspond to the exhaustively studied one-component plasma and hard-sphere systems.

A natural time scale is provided by τ_E, the period of an Einstein oscillator in a crystal. The Einstein periods for the fcc and bcc phases change by an order of magnitude over the range of λ studied here $(3\leqslant\lambda\leqslant 8)$, yet differ from each other by less than 1.2% at any given λ within this range. To obtain consistent results across a wide range of screening lengths, we normalize all time scales in this study to $\tau_E(\lambda)$, using the fcc values given in Ref. [21].

A natural energy scale is given by the Einstein phonon energies $m\omega_E^2a^2$, where m is the macroion mass and $\omega_E=2\pi/\tau_E$ is the Einstein frequency. Following Kremer *et al.* [20], we define the dimensionless temperature

$$\tilde{T}=\frac{k_BT}{m\omega_E^2a^2} \tag{4}$$

using the fcc phonon energies, and plot our phase diagram in $(\lambda,\tilde{T})$ space. A dimensionless inverse temperature $\Gamma=(\Phi/a)/k_BT$ called the coupling parameter is used in many studies of dusty plasmas. The advantage of using $\tilde{T}$ rather than Γ in Yukawa phase diagrams is that the transition lines are approximately linear in λ.

The bcc and fcc phases coexist in equilibrium over a part of the phase diagram. Following previous authors [20–23], we define the bcc-fcc transition line as the curve $\tilde{T}_{trans}(\lambda)$ on which $\Delta F=\Delta F(\lambda,\tilde{T})=0$. This transition line will certainly lie within the coexistence region, regardless of the thermodynamic state dependence of κ and Φ. We find $\tilde{T}_{trans}(\lambda)$ by calculating ΔF at many points $(\lambda_i,\tilde{T}_i)$ on the phase diagram.

C. MD simulation details

We simulate N-V-T ensembles of identical particles using a velocity-Verlet [37] algorithm to integrate the particle trajectories. The temperature is maintained with a Langevin thermostat [38]. Periodic boundary conditions are used to maintain the density. The equations of motion for the position $\vec{q}_i$ and peculiar momentum $\vec{p}_i$ of the ith particle are

$$\dot{\vec{q}}_i=\vec{p}_i/m+\dot{\overline{\epsilon}}\vec{q}_i, \tag{5}$$

$$\dot{\vec{p}}_i=\vec{F}_i-\dot{\overline{\epsilon}}\vec{p}_i+\vec{\eta}_i-\vec{p}_i/\tau_{Lang}, \tag{6}$$

where $\dot{\overline{\epsilon}}$ is the true strain-rate tensor, $\vec{F}_i$ is the force due to Yukawa interactions, $\vec{\eta}_i$ is a random noise term, and τ_{Lang} is the characteristic relaxation time of the thermostat. We use a time step $\delta t=0.01\tau_E$ to ensure proper integration of Eqs. (5) and (6) and set $\tau_{Lang}=10\tau_E$. Changing δt and τ_{Lang} by a factor of 2 in either direction had no effect on the phase diagram.

For numerical efficiency we truncate interactions at a cutoff radius r_c. Due to the presence of long range order in Yukawa crystals, care must be taken in choosing this cutoff radius. We present the details of our determination of $r_c(\lambda)$ in Sec. III B.

In most of our simulations, we impose the bcc$\rightarrow$fcc Bain transformation as follows. We start with a lattice of 3456 particles (12^3 bcc unit cells) in a cubic simulation cell with edges of length $L_x=L_y=L_z=L_0$ aligned with the $\langle 100\rangle$ directions of the lattice. The system is equilibrated for 200 Einstein periods. We then fix $\dot{\zeta}=\dot{L}_z/L_0$ for a time Δt sufficient to reach the fcc structure: $\Delta t=(2^{1/3}-1)\dot{\zeta}^{-1}$. The other cell edges L_x and L_y are varied to maintain constant volume and tetragonality ($L_x=L_y=\sqrt{L_0^3/L_z}$). The true strain-rate tensor $\dot{\overline{\epsilon}}$ is then given by

$$\dot{\epsilon}_{zz}=\dot{L}_z/L_z=\dot{\zeta}/\zeta, \tag{7}$$

$$\dot{\epsilon}_{xx}=\dot{\epsilon}_{yy}=\dot{L}_x/L_x=-\dot{\zeta}/2\zeta, \tag{8}$$

$$\dot{\epsilon}_{xy}=\dot{\epsilon}_{xz}=\dot{\epsilon}_{yz}=0. \tag{9}$$

We compute the diagonal elements (P_x,P_y,P_z) of the pressure tensor using standard methods [39]. Equation (1) then takes on the more physically familiar form

$$W_{bf}=-\int_0^{\Delta t}(P_xL_yL_z\dot{L}_x+P_yL_xL_z\dot{L}_y+P_zL_xL_y\dot{L}_z)dt. \tag{10}$$

After the system has reached the fcc structure, the deformation process is reversed by changing the sign of $\dot{\zeta}$. As the system returns to bcc, W_{fb} is calculated using the analog of Eq. (10).

To minimize uncertainties in $\tilde{T}_{trans}(\lambda)$, $\dot{\zeta}$ must be small enough for the system to remain near equilibrium. One requirement is that the strain-rate components $(\dot{\overline{\epsilon}}\vec{q}_i)$ of the velocities must be small compared to the thermal velocity. The Bain transformation time Δt (which is proportional to $\dot{\zeta}^{-1}$) must also be large compared to τ_{Lang} to allow the thermostat to transfer heat to or away from the system as necessary to maintain constant temperature. Since τ_{Lang} sets the time over which the system samples the canonical ensemble, the thermodynamic sampling improves as $\Delta t/\tau_{Lang}$ increases.

The precision of the calculated transition line depends on the difference $(\Delta F_{max}-\Delta F_{min})\equiv W_{bf}+W_{fb}=W_{cycle}$ between the bounds on ΔF. These bounds converge to each other in the reversible thermodynamic (zero strain-rate) limit. In this limit, the average work $\langle W_{cycle}\rangle$ done on the system over a full deformation cycle (bcc$\rightarrow$fcc$\rightarrow$bcc or vice versa) should vanish. In simulations at finite strain rate, however, there is a positive systematic error in W_{cycle} due to energy dissipation [40]. This can be physically interpreted as arising from viscosity. Each applied strain increment takes the system slightly out of equilibrium. When $\dot{\zeta}$ is small, one expects the stresses to deviate from their equilibrium values by an amount $\overline{\sigma}_{visc}\sim\dot{\zeta}$ [41]. Sources of viscous dissipation include the intrinsic viscosity and the drag forces $-\vec{p}_i/\tau_{Lang}$ on the particles applied by the Langevin thermostat. The viscous dissipation rate is given by $\overline{\sigma}_{visc}\cdot\dot{\overline{\epsilon}}$, so one expects the dissipated power to be proportional to $\dot{\zeta}^2$. Since the total simulation time scales as $\dot{\zeta}^{-1}$, the total dissipated energy, and hence the deviation of $\langle W_{cycle}\rangle$ from zero, should be linearly proportional to $\dot{\zeta}$. We present the $\dot{\zeta}$ dependence of our results in Sec. III A.

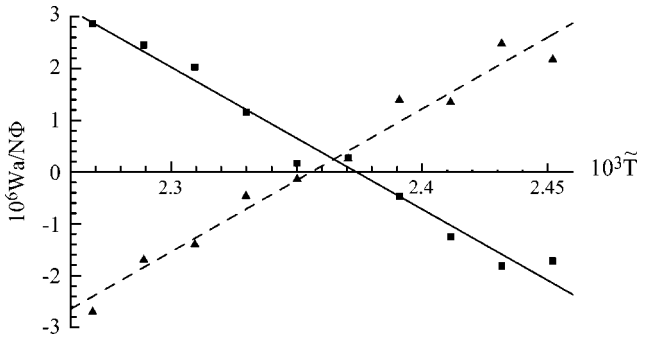

FIG. 2. Simulation results for $\lambda=5, \dot{\zeta}=10^{-4}/\tau_E$. Solid triangles are values of W_{bf}, solid squares are values of W_{fb}. The dashed and solid lines are linear fits to the results. $\tilde{T}_{bf}$ and $\tilde{T}_{fb}$ are the intersections of these lines with $W=0$.

III. RESULTS

A. Strain-rate dependence

At temperatures near the transition line, calculations of the geometrical structure factor and pair correlation function verify that our systems traverse the Bain transformations homogeneously. This homogeneity allows us to use Eqs. (1) and (2) for calculating W_{bf} and W_{fb} and leads to tight bounds on ΔF.

We obtained results similar to those shown in Fig. 2 over the entire investigated range of λ and for three different values of $\dot{\zeta}$. Near the transition line, $W_{bf}(\lambda,\tilde{T})$ and $W_{fb}(\lambda,\tilde{T})$ vary linearly with $\tilde{T}$ and have nearly opposite (λ-dependent) slopes. The scatter about linear fits to $W_{bf}(\lambda,\tilde{T})$ and $W_{fb}(\lambda,\tilde{T})$ is consistent with fluctuations in W_{bf} and W_{fb} at fixed $(\lambda,\tilde{T})$. The intersections of these fits with $W=0$ give two estimates, $\tilde{T}_{bf}$ and $\tilde{T}_{fb}$, for $\tilde{T}_{trans}$. These are obtained using data at ten evenly spaced $\tilde{T}$ within about 5% of the transition line.

For a given system, $\tilde{T}_{fb}$ and $\tilde{T}_{bf}$ provide upper and lower bounds on $\tilde{T}_{trans}$ since $W_{bf}>\Delta F>-W_{fb}$ and $(\partial\Delta F/\partial\tilde{T})>0$. We define the fractional uncertainty due to dissipative hysteresis as

$$\delta_{hyst}=(\tilde{T}_{fb}-\tilde{T}_{bf})/(\tilde{T}_{fb}+\tilde{T}_{bf}). \tag{11}$$

The conditions $\delta_{hyst}\sim\dot{\zeta}$ and $\langle W_{cycle}\rangle\sim\dot{\zeta}$ are equivalent due to the linear dependence of W_{bf} and W_{fb} on $\tilde{T}$. Figure 3 shows the $\dot{\zeta}$ dependence of δ_{hyst} for $\lambda=4$ and $\lambda=5$. The results are

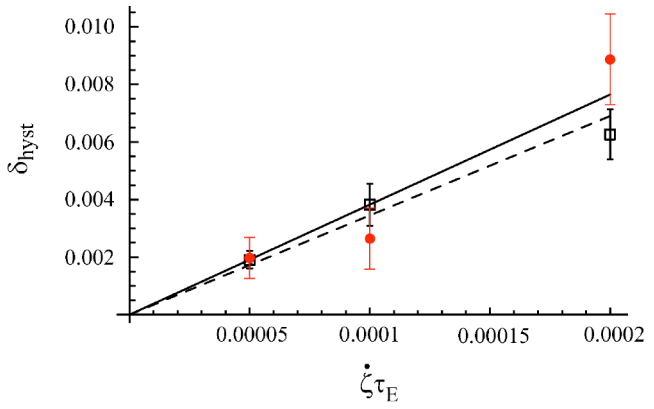

FIG. 3. (Color online) Strain-rate dependence of δ_{hyst}. Solid circles indicate $\lambda=4$ results. Empty squares indicate $\lambda=5$ results. The solid and dashed lines are linear fits to the data. The error bars indicate statistical uncertainties.

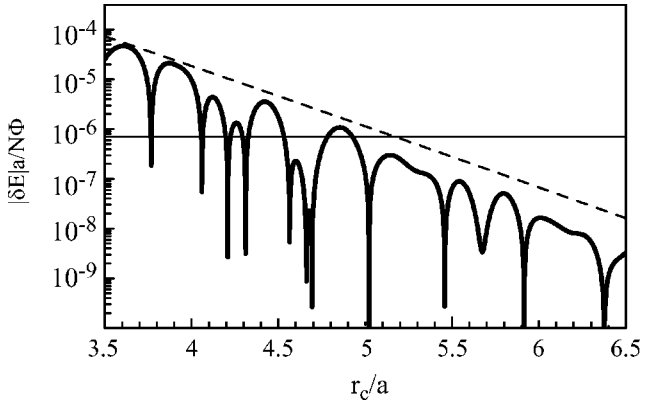

FIG. 4. Determination of r_c for $\lambda=3$. The heavy curve is our estimate of $\delta E(r_c)$ obtained from simulations at $\tilde{T}=8.84\times10^{-3}$, with $r_l=10a$. The dashed line is the analytic upper bound on $\delta E(r_c)$ from Eq. (14) with $\Omega=1/3$. The horizontal line is the value of $|\delta E|$ in Eq. (12) corresponding to $|\delta_{cut}|=0.01$.

consistent with our hypothesis that the energy dissipated is linear in $\dot{\zeta}$.

We identify $\tilde{T}_{trans}=(\tilde{T}_{bf}+\tilde{T}_{fb})/2$ as the best estimate for the transition temperature for a given system size, system geometry, and potential cutoff radius. Table I shows that the fractional variation of $\tilde{T}_{trans}$ with $\dot{\zeta}$ is much smaller than δ_{hyst} [42].

In the following, we present results for $|\dot{\zeta}|=10^{-4}/\tau_E$. Based on Table I, for this value of $|\dot{\zeta}|$ the random and finite strain-rate uncertainties in $\tilde{T}_{trans}$ are comparable, both about 0.2%. The combined error is estimated to be less than 0.4%. The uncertainties given in subsequent tables include only statistical uncertainties from the linear fits used to calculate $\tilde{T}_{bf}$ and $\tilde{T}_{fb}$.

B. Potential cutoff dependence

We estimate the errors introduced by truncating the force at r_c by calculating the error $\delta E(r_c)$ in the potential energy difference. If the error in ΔF is of the same order, then the fractional error in the transition temperature is

$$\delta_{cut}\equiv\frac{\delta\tilde{T}(r_c)}{\tilde{T}}\simeq\frac{1}{\tilde{T}}\frac{\partial\tilde{T}}{\partial\Delta F}\delta E(r_c). \tag{12}$$

Here $(\partial\tilde{T}/\partial\Delta F)$ is known near the transition line from the work calculations.

TABLE I. Dependence of $\tilde{T}_{trans}(\lambda)$ on dimensionless strain rate.

$\dot{\zeta}\tau_E$	$10^3\tilde{T}_{trans}$ ($\lambda=4$)	$10^3\tilde{T}_{trans}$ ($\lambda=5$)
5×10^{-5}	1.637±0.003	2.363±0.002
1×10^{-4}	1.634±0.004	2.365±0.004
2×10^{-4}	1.633±0.005	2.366±0.005

The cutoff-induced error in the potential energy difference can be written in terms of the pair correlation functions $g_{fcc}(r)$ and $g_{bcc}(r)$ of the fcc and bcc crystals. For N particles

$$\delta E(r_c)=\frac{N}{2}\int_{r_c}^{\infty}U(r)[g_{fcc}(r)-g_{bcc}(r)]4\pi r^2dr/a^3. \tag{13}$$

If $\Omega\equiv\max\{|g_{fcc}(r)-g_{bcc}(r)|,\quad r\geq r_c\}$, then

$$\frac{|\delta E(r_c)|}{N(\Phi/a)}<\frac{\Omega}{\Phi a^2}\int_{r_c}^{\infty}U(r)2\pi r^2dr=\frac{2\pi\Omega(1+\lambda r_c/a)e^{-\lambda r_c/a}}{\lambda^2}. \tag{14}$$

One expects Ω to be of order 1 at finite temperature.

For $\lambda=3,4$, and 5, we estimated $\delta E(r_c)$ at $\tilde{T}\simeq\tilde{T}_{trans}$ by calculating the pair correlation functions in large systems using large cutoff radii and long integration times. Due to the exponential falloff of $U(r)$ and finite temperature smoothing of $g(r)$, the infinite upper bound in Eq. (13) can be replaced by a finite value r_l without introducing significant errors. We found $\lambda r_l=30a$ to be sufficiently large.

Figure 4 shows our estimate of $|\delta E(r_c)/(N\Phi/a)|$ from Eq. (13) and the value of $|\delta E/(N\Phi/a)|$ corresponding to $\delta_{cut}=0.01$ for $\lambda=3$, the longest-range potential considered. We found that Ω decreases from 1.4 to 0.62 as r_c increases from $3.5a$ to $6.5a$. The actual error is always smaller than the bound given by Ω because $g_{fcc}-g_{bcc}$ oscillates in sign. The envelope shown corresponds to $\Omega=1/3$. Because of the sharp variation of $\delta E(r_c)$, we use this envelope to estimate δ_{cut}.

To test Eq. (12) we calculated $\tilde{T}_{trans}$ as a function of r_c for $\lambda=3$. Results are shown in Table II. The fractional changes in $\tilde{T}_{trans}$ from $r_c=3.5a$ to $r_c=6.667a$ and from $r_c=4.667a$ to $r_c=6.667a$ are 19% and 0.9%, respectively. Both changes are about one fifth of the estimates for δ_{cut} from Eqs. (12) and (13). No statistically significant changes are expected or ob-

TABLE II. $\tilde{T}_{trans}$ vs r_c for $\lambda=3$. $|\delta_{cut}|$ is given by Eq. (12) and the bound in Eq. (14).

r_c	$\lvert\delta_{cut}\rvert$	$10^3\tilde{T}_{trans}$
$3.5a$	1.04	1.048 ± 0.003
$4.667a$	0.041	0.871 ± 0.002
$5.833a$	0.0015	0.880 ± 0.002
$6.667a$	0.00014	0.879 ± 0.003

served for $r_c \geq 5.833a$. We conclude that errors estimated from the envelopes of curves like Fig. 4 give a conservative estimate of cutoff errors.

To ensure that the fractional systematic errors were no larger than our random and rate errors, we chose r_c slightly above the values corresponding to $|\delta_{cut}|=0.002$. For $\lambda=3,4$, and 5, we used cutoff radii of $5.833a$, $4.375a$, and $3.5a$ in the simulations used to determine $\tilde{T}_{trans}$. Smaller r_c can be used at higher λ both because the interactions weaken and $\tilde{T}_{trans}/\tilde{T}_{melt}$ increases, leading to a smaller Ω. For $\lambda \geq 5$ we fixed the cutoff radius at $r_c=3.5a$.

C. System size and geometry dependence

To examine finite-size effects we also considered a 432-particle system (initial state 6^3 bcc unit cells). Because the corresponding fcc state has transverse length $6.73a$, the minimum image convention requires $r_c < 3.367a$, and we used $r_c=3.3a$. To separate out r_c dependence from system size dependence, we also recalculated the transition line for $N=3456$ for $5 \leq \lambda \leq 8$ with $r_c=3.3a$.

Table III shows a comparison of our calculated transition temperatures. The $N=432$ values were systematically lower, but the effect was small. From theoretical considerations one expects the leading finite size corrections to $\Delta F/N$ to be proportional to $1/N$ [43]. This should produce a corresponding error in $\tilde{T}_{trans}$. As shown in Table III, the changes in $\tilde{T}_{trans}$ from $N=432$ to $N=3456$ were all about 1%. The changes in $\tilde{T}_{trans}$ from $N=3456$ to $N=\infty$ for this system geometry should be about eight times smaller.

Another test indicates that finite-size effects are larger than the above estimate. The geometry was changed so that the fcc state has equal cell edges and the bcc state has $L_x=L_y=\sqrt{2}L_z$. These simulations contained 10^3 fcc unit cells (4000 particles) with the $\langle 100\rangle$ directions parallel to the simulation cell edges. After Bain transformation, the bcc state has two $\langle 110\rangle$ directions parallel to the simulation cell edges. As shown in Table IV, the values of $\tilde{T}_{trans}$ obtained for both $\lambda=4$ and $\lambda=7$ were 0.6% lower than those obtained with the standard system geometry [44]. Other simulations verified that this was due solely to the change in boundary conditions. We conclude that our dominant source of uncertainty is finite size and is less than 1%.

TABLE III. Dependence of $\tilde{T}_{trans}$ on N.

λ	$10^3\tilde{T}_{trans}$ ($N=432$)	$10^3\tilde{T}_{trans}$ ($N=3456$)
5	2.350 ± 0.009	2.362 ± 0.004
6	2.985 ± 0.011	3.021 ± 0.003
7	3.562 ± 0.009	3.593 ± 0.005
8	4.064 ± 0.008	4.087 ± 0.005

TABLE IV. Dependence of $\tilde{T}_{trans}$ on system geometry.

λ	$10^3\tilde{T}_{trans}$ ($N=3456$)	$10^3\tilde{T}_{trans}$ ($N=4000$)
4	1.634 ± 0.004	1.625 ± 0.004
7	3.592 ± 0.004	3.570 ± 0.004

We attribute the observed sensitivity to geometry to the change in allowed low-frequency modes. These modes play a disproportionate role in determining the entropy in lattice dynamics calculations [45] and drive the fcc$\rightarrow$bcc transition with increasing temperature [21]. Since the shear velocity is highly anisotropic in the bcc phase, changing the boundaries affects the sampling of these low-frequency modes and thus ΔF.

D. Transition line

Table V shows our calculated $\tilde{T}_{trans}(\lambda)$ with statistical uncertainties. As described above, the combined systematic errors due to finite strain rate, system size, and potential cutoff are estimated to be less than 1%. Results of a cubic polynomial fit to the data are also given:

$$10^4\tilde{T}^{fit}_{trans}(\lambda) = 6.466\,78(\lambda-\lambda_0) + 0.430\,01(\lambda-\lambda_0)^2 - 0.068\,06(\lambda-\lambda_0)^3, \quad (15)$$

where $\lambda_0=1.718$ is the zero-temperature transition point obtained from lattice statics calculations [46]. Lower-order polynomials fail to adequately fit the data within our uncertainties.

Figure 5 shows the polynomial fit and two previously published solid-fluid coexistence lines [17,23]. The intersections of these lines give estimated values of the bcc-fcc-fluid triple point. Using results from Ref. [17] we find ($\lambda_{tp}=7.45, \tilde{T}_{tp}=0.003\,84$). Those from Ref. [23] yield ($\lambda_{tp}=7.84, \tilde{T}_{tp}=0.004\,01$).

TABLE V. Calculated and fit values of $\tilde{T}_{trans}$. Only statistical uncertainties are quoted.

λ	$10^3\tilde{T}_{trans}$	$10^3\tilde{T}^{fit}_{trans}$
3	0.880 ± 0.002	0.885
4	1.634 ± 0.004	1.619
5	2.365 ± 0.004	2.345
6	3.017 ± 0.004	3.023
7	3.592 ± 0.004	3.613
8	4.085 ± 0.004	4.072

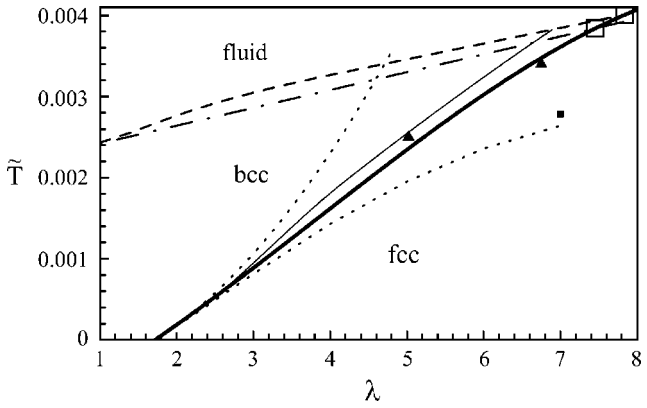

FIG. 5. Phase diagram of Yukawa systems. The heavy line is our cubic polynomial fit for the bcc-fcc transition line. The light solid line is the fcc-bcc transition line from Ref. [23]. The lower and higher dotted lines are, respectively, the lattice dynamics and molecular dynamics bcc-fcc transition lines from Ref. [21]. The triangles are a bcc-fcc coexistence point and triple point from Ref. [22], and the solid square is a bcc-fcc transition point from Ref. [24]. The dashed and dash-dotted lines are the melting lines from Ref. [17,23]. The empty squares denote our estimates for the bcc-fcc-fluid triple point.

If we assume that the parameters κ and Φ are density independent, we can calculate the width of the bcc-fcc coexistence region from the pressures and bulk moduli of the two phases on the line where $\Delta F=0$. The bcc pressure is larger than the fcc pressure by only about 0.04% for $\lambda=4$, and by 0.65% for $\lambda=7$. This results in a higher density in the fcc phase at coexistence, but only by about 0.015% at $\lambda=4$ and 0.2% at $\lambda=7$. The corresponding changes in λ and $\tilde{T}$ are much smaller than the uncertainties in our calculated transition line. The coexistence region in experimental systems may be much larger due to variations in κ and Φ with density [26,29]. As noted above, these variations are system specific and a more complete treatment is beyond the scope of this paper.

E. Anharmonic effects

The lower dotted line in Fig. 5 shows lattice dynamics results for the bcc-fcc transition line [21]. In this approximation the energy and entropy differences, ΔE_{LD} and ΔS_{LD}, are independent of T. The fcc-bcc transition line is given by $T_{LD}=\Delta E_{LD}/\Delta S_{LD}$. The resulting curve lies below $\tilde{T}_{trans}$, indicating that the fcc phase is stabilized by anharmonic effects [21,23]. This implies that the anharmonic component of the free energy difference,

$$\Delta F_{an} \equiv \Delta E_{an} - T\Delta S_{an} = \Delta F - \Delta F_{LD}, \tag{16}$$

is negative on the transition line. The relative signs and magnitudes of ΔE_{an} and ΔS_{an} may be calculated by comparing our accurate measurements of free and total energy differences with the lattice-dynamics results.

Table VI shows results for anharmonic contributions to the free and total energy differences on the fit transition line [47]. The values of ΔF_{an} are known from the work calculations, while the values of ΔE_{an} were found from separate equilibrium simulations. The anharmonic corrections to the total energy favor the bcc phase for all λ, i.e., $E_{fcc}-E_{bcc}$ on the transition line has increased relative to its zero-temperature value. The anharmonic contributions to the free energy difference, however, are larger in magnitude and opposite in sign, implying that anharmonic entropic contributions to ΔF favor the fcc phase at all λ and overwhelm energetic contributions.

TABLE VI. Anharmonic free and total energy differences evaluated at $\tilde{T}^{fit}_{trans}(\lambda)$.

λ	$10^2\Delta F_{an}/Nk_BT$	$10^2\Delta E_{an}/Nk_BT$
3	-0.58 ± 0.1	0.42 ± 0.33
4	-1.07 ± 0.12	1.0 ± 0.4
5	-1.92 ± 0.15	1.2 ± 0.4
6	-3.03 ± 0.17	2.4 ± 0.4
7	-4.33 ± 0.21	2.2 ± 0.4

In lattice calculations the larger entropy of the bcc phase comes mainly from the lower frequency of its shear modes. Some of these modes have negative energy for $\lambda>7.67$, causing the bcc phase to become linearly unstable at low temperatures [21]. It is interesting that the onset of this low-temperature instability is close to λ_{tp}. However, we have performed runs near the melting line for λ as large as 10 and find that the bcc phase remains metastable. This implies that anharmonic effects have increased the frequency of long wavelength shear modes, providing an explanation for the decreased entropy advantage of the bcc phase.

IV. COMPARISON TO PREVIOUS RESULTS

Miller and Reinhardt were the first authors to use Bain deformation paths to obtain bounds on ΔF for Yukawa systems [24]. They calculated the work by integrating the change in the Hamiltonian rather than from the stresses and strains. The large discrepancy between their $\lambda=7$ transition temperature and our result is likely due to their extremely small system size ($N=108$), which was just used to illustrate their method.

The earliest MD calculations [20,21] of the transition line also deviate substantially from ours, particularly at large λ. The upper dotted line shown in Fig. 5 is a fit between points where the fcc and bcc phases were found to be stable. The gap between points was about 20% and the final shape was strongly influenced by a bcc-stable point above the melting line. Other points where the bcc phase was stable lie close to our $\tilde{T}_{trans}$ but are shifted up due to the smaller r_c used.

Our transition line is in qualitative agreement with more recent MD and Monte Carlo results [22,23]. Dupont *et al.* calculated a fcc-bcc coexistence point and the fcc-bcc-fluid triple point using small systems ($N\simeq250$). Although their triple point ($\lambda_{tp}=6.75, \tilde{T}_{tp}=0.0034$) lies well below ours ($\lambda_{tp}=7.7\pm0.3, \tilde{T}_{tp}=0.0039\pm0.0001$) and well below recently

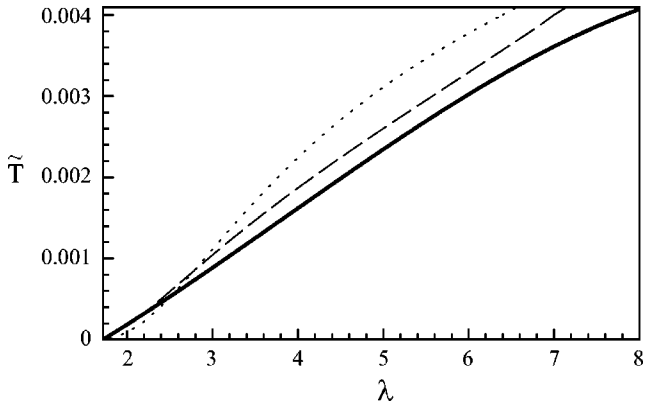

FIG. 6. Comparison of transition line to analytic estimates. The heavy line is our $\tilde{T}^{fit}_{trans}(\lambda)$. The dashed and dotted lines are the analytic estimates for the bcc→fcc and fcc→bcc transitions from Ref. [10].

published melting lines [17,23], it lies only about 2% below our fcc-bcc transition line.

Hamaguchi, *et al.* also obtain a lower triple point ($\lambda_{tp}=6.90, \tilde{T}_{tp}=0.0038$) because their bcc-fcc transition temperatures are systematically (6–10%) higher than ours [23]. One possible explanation is that their equilibration times were too short. They used the λ-independent time unit $\tau=\sqrt{3}\omega_p^{-1}$, where $\omega_p=\sqrt{4\pi n\Phi/m}$ is the plasma frequency. Starting with perfect bcc and fcc lattices as their initial conditions, they equilibrated their systems for a maximum of 300 τ before beginning their free energy measurements. This corresponds to about $27\tau_E$ for $\lambda=3$ and only $4\tau_E$ for $\lambda=8$. Since the latter is only about four times the velocity autocorrelation time, and comparable to the time for sound to propagate across their simulation cells, it is doubtful that their systems had equilibrated sufficiently at high λ. Too short an equilibration time could cause overestimation of the stability of the phase with lower entropy, the fcc phase, which is consistent with their findings.

Vaulina and colleagues have proposed phenomenological criteria for the bcc-fcc transition [10]. They assume that κ^{-1} is an effective hard-sphere radius and predict that the value of the rms displacement at the fcc transition Δ_{trans} satisfies

$$2(1-\pi\sqrt{2}/6)^{-1/3}\Delta_{trans}=R_{WS}-\kappa^{-1}, \tag{17}$$

where $R_{WS}=(4\pi/3)^{-1/3}a$ is the Wigner-Seitz radius. They then use an approximate formula for the effective frequency in an Einstein-like model to determine Δ for the fcc and bcc structures. These values of Δ give two predictions for the transition line. As shown in Fig. 6, their predictions are qualitatively correct but lie roughly 10–40% above our $\tilde{T}_{trans}$.

The discrepancy in Fig. 6 could be due to a failure either of Eq. (17) or of the approximations used to find Δ. To test this we performed equilibrium simulations at $\tilde{T}^{fit}_{trans}$ in both bcc ($N=3456$) and fcc ($N=4000$) systems. Our results for the rms displacements, Δ_{fcc} and Δ_{bcc}, are compared to the predictions of Eq. (17) in Table VII. The rms displacements for the fcc structure lie quite close to the prediction for small λ, and about 13% above it at $\lambda=7$. Finite size effects decrease Δ_{fcc} relative to the $N=\infty$ value [45,48]. These results indicate that most of the error in the transition lines of Vaulina *et al.* comes from substantial underestimation of the rms displacements. They calculate Δ in the harmonic approximation, and anharmonic corrections increase Δ for these λ [21]. Note that the measured bcc displacements in Table VII are larger due to the bcc lattice's softer shear modes [21].

TABLE VII. Rms displacements at $\tilde{T}^{fit}_{trans}(\lambda)$. Δ_{trans} is the prediction from Eq. (17), while Δ_{fcc} and Δ_{bcc} are results from equilibrium MD simulations.

λ	Δ_{trans}/a	Δ_{fcc}/a	Δ_{bcc}/a
3	0.0915	0.089	0.096
4	0.1181	0.118	0.128
5	0.1341	0.140	0.154
6	0.1447	0.159	0.177
7	0.1522	0.171	0.192

V. SUMMARY AND CONCLUSIONS

We calculated the bcc-fcc coexistence line of Yukawa systems to an uncertainty of approximately 1% through integration of the mechanical work along Bain transformation paths. The range of bcc stability was found to be slightly greater than that found in previous comprehensive studies [21–23], and the triple point shown to lie at higher inverse screening length. The large changes in $\tilde{T}_{trans}$ with r_c for small λ indicate that the relative stability of fcc and bcc phases depends sensitively on long-range correlations, and calls into question the use of local nearest-neighbor arguments to calculate the transition line. Nevertheless, we found that one such phenomenological criterion [10], derived from the idea that the fcc phase is stable when interparticle interactions are hard-sphere-like [49], predicts the transition line remarkably well when combined with MD results for the mean-squared displacement.

Comparison with lattice-dynamics results shows that anharmonic terms in the total energy favor the bcc phase for all λ, but that these corrections are overbalanced by anharmonic contributions to the entropy. The change in entropy appears to reflect an increase in the frequency of long-wavelength shear modes in the bcc phase. This increase also stabilizes the bcc phase against a linear shear instability observed for $\lambda>7.67$ at low $\tilde{T}$.

We found that shifts in the transition line due to finite-size effects are less than 1% if $N\sim3000-4000$, but that the presence of long-range order at temperatures near the transition line in weakly screened systems requires a cutoff radius larger than that used in some previous studies [20,21]. Accurate simulations of weakly screened ($\lambda<3$) systems in this temperature range require either larger system sizes or an Ewald-like summation over periodic images [23]. However, we have also shown that a reasonably small potential cutoff

need not introduce large errors in a transition line calculation in the moderate-screening regime, provided the cutoff is chosen with some care.

It is known that the phase behavior of real systems such as charge-stabilized colloidal suspensions is not fully described by pointlike Yukawa interactions. Recent simulations of charged macroions in a dynamic neutralizing background have shown that the repulsive interactions between macroions are truncated by many-body effects, destabilizing the crystalline phases in the weak screening limit [50–52]. Direct, hard-core repulsions also significantly alter the phase diagram when the volume fraction is more than a few percent [53–55]. However, we hope that our high-precision calculation of the point Yukawa fcc-bcc transition line may serve as a benchmark for further studies of more sophisticated models.

ACKNOWLEDGMENTS

The simulations in this paper were carried out using the LAMMPS molecular dynamics software (http://www.cs.sandia.gov/~sjplimp/lammps.html). Support from NSF Grant No. DMR-0083286 is gratefully acknowledged.

[1] N. W. Ashcroft and N. D. Mermin, *Solid State Physics* (Saunders, Philadelphia, 1976).
[2] E. C. Whipple, T. Northrop, and D. Mendis, J. Geophys. Res., [Space Phys.] **90** (A8), 7405 (1985).
[3] S. Hamaguchi and R. T. Farouki, J. Chem. Phys. **101**, 9876 (1994).
[4] Y. Rosenfeld, Phys. Rev. E **49**, 4425 (1994).
[5] E. Verwey and J. T. G. Overbeek, *Theory of the Stability of Lyophilic Colloids* (Elsevier, New York, 1948).
[6] S. Alexander, P. Chaikin, P. Grant, G. J. Morales, and P. Pincus, J. Chem. Phys. **80**, 5776 (1984).
[7] M. J. Stevens, M. L. Falk, and M. O. Robbins, J. Chem. Phys. **104**, 5209 (1996).
[8] T. Palberg, W. Monch, F. Bitzer, R. Piazza, and T. Bellini, Phys. Rev. Lett. **74**, 4555 (1995).
[9] W.-H. Shih and D. Stroud, J. Chem. Phys. **79**, 6254 (1983).
[10] O. S. Vaulina, S. V. Vladimirov, O. F. Petrov, and V. E. Fortov, Phys. Rev. Lett. **88**, 245002 (2002).
[11] D. Hone, S. Alexander, P. Chaikin, and P. Pincus, J. Chem. Phys. **79**, 1474 (1983).
[12] C. F. Tejero, J. F. Lutsko, J. L. Colot, and M. Baus, Phys. Rev. A **46**, 3373 (1992).
[13] O. S. Vaulina, J. Exp. Theor. Phys. **94**, 26 (2002).
[14] R. O. Rosenberg and D. Thirumalai, Phys. Rev. A **36**, 5690 (1987).
[15] E. J. Meijer and D. Frenkel, J. Chem. Phys. **94**, 2269 (1991).
[16] J. C. Zahorchak, R. Kesavamoorthy, R. D. Coalson, and S. A. Asher, J. Chem. Phys. **96**, 6873 (1992).
[17] M. J. Stevens and M. O. Robbins, J. Chem. Phys. **98**, 2319 (1993).
[18] R. T. Farouki and S. Hamaguchi, J. Chem. Phys. **101**, 9885 (1994).
[19] S. Hamaguchi, R. T. Farouki, and D. H. E. Dubin, J. Chem. Phys. **105**, 7641 (1996).
[20] K. Kremer, M. O. Robbins, and G. S. Grest, Phys. Rev. Lett. **57**, 2694 (1986).
[21] M. O. Robbins, K. Kremer, and G. S. Grest, J. Chem. Phys. **88**, 3286 (1988).
[22] G. Dupont, S. Moulinasse, J. P. Ryckaert, and M. Baus, Mol. Phys. **79**, 453 (1993).
[23] S. Hamaguchi, R. T. Farouki, and D. H. E. Dubin, Phys. Rev. E **56**, 4671 (1997).
[24] M. A. Miller and W. P. Reinhardt, J. Chem. Phys. **113**, 7035 (2000).
[25] J. H. Chu and L. I, Phys. Rev. Lett. **72**, 4009 (1994).
[26] A. P. Nefedov *et al.*, New J. Phys. **5**, 33 (2003).
[27] Y. Monovoukas and A. P. Gast, J. Colloid Interface Sci. **128**, 533 (1989).
[28] E. B. Sirota, H. D. Ou-Yang, S. K. Sinha, P. M. Chaikin, J. D. Axe, and Y. Fujii, Phys. Rev. Lett. **62**, 1524 (1989).
[29] H. Schope, T. Decker, and T. Palberg, J. Chem. Phys. **109**, 10068 (1998).
[30] κ typically depends explicitly on the densities of the mobile counterions that screen interactions between macroions. These densities change with macroion density to maintain charge neutrality.
[31] T. P. Straatsma, H. J. C. Berendsen, and J. P. M. Postma, J. Chem. Phys. **85**, 6720 (1986).
[32] W. P. Reinhardt and J. E. Hunter, J. Chem. Phys. **97**, 1599 (1992).
[33] J. E. Hunter, W. P. Reinhardt, and T. F. Davis, J. Chem. Phys. **99**, 6856 (1993).
[34] F. Reif, *Fundamentals of Statistical and Thermal Physics* (McGraw-Hill, New York, 1965).
[35] F. Milstein, H. E. Fang, and J. Marschall, Philos. Mag. A **70**, 621 (1994).
[36] W. G. Hoover, D. J. Evans, R. B. Hickman, A. J. C. Ladd, W. T. Ashurst, and B. Moran, Phys. Rev. A **22**, 1690 (1980).
[37] W. C. Swope, H. C. Andersen, P. H. Berens, and K. Wilson, J. Chem. Phys. **76**, 637 (1982).
[38] T. Schneider and E. Stoll, Phys. Rev. B **17**, 1302 (1978).
[39] M. P. Allen and D. J. Tildesly, *Computer Simulation of Liquids* (Clarendon, Oxford, 1987).
[40] C. Jarzynski, Phys. Rev. Lett. **78**, 2690 (1997).
[41] R. G. Larson, *The Structure and Rheology of Complex Fluids* (Oxford University Press, New York, 1999).
[42] These values are for the standard system size and geometry described in Sec. II C and cutoff radii reported in Sec. III B.
[43] J. M. Polson, E. Trizac, S. Pronk, and D. Frenkel, J. Chem. Phys. **112**, 5339 (2000).

[44] Both sets of simulations used the cutoff radii indicated in Sec. III B.
[45] M. O. Robbins, G. S. Grest, and K. Kremer, Phys. Rev. B **42**, 5579 (1990).
[46] J. Medeiros e Silva and B. J. Mockross, Phys. Rev. B **21**, 2972 (1980).
[47] Results for $\lambda=8$ are not presented in Table VI and VII, respectively, because at $\tilde{T}_{trans}$ solid diffusion prohibits accurate calculations of the rms displacements, and lattice dynamics calculations of ΔS diverge.
[48] Equilibrium simulations of larger ($N \simeq 100\,000$) systems for $\lambda=5$ showed that both Δ_{fcc} and Δ_{bcc} increase with N, worsening the agreement with Δ_{trans}, but that the finite-size corrections are small compared to the discrepancies shown in Table VII.
[49] W. G. Hoover and F. H. Ree, J. Chem. Phys. **49**, 3609 (1968).
[50] J. Dobnikar, R. Rzehak, and H. H. von Grunberg, Europhys. Lett. **61**, 695 (2003).
[51] J. Dobnikar, Y. Chen, R. Rzehak, and H. H. von Grunberg, J. Chem. Phys. **119**, 4971 (2003).
[52] A. P. Hynninen and M. Dijkstra, J. Phys.: Condens. Matter **15**, 3557 (2003).
[53] E. J. Meijer and F. E. Azhar, J. Chem. Phys. **106**, 4678 (1997).
[54] A. P. Hynninen and M. Dijkstra, Phys. Rev. E **68**, 021407 (2003).
[55] F. E. Azhar, M. Baus, J. Ryckaert, and E. Meijer, J. Chem. Phys. **112**, 5121 (2000).